Innate-like gene expression of lung-resident memory CD8+ T-cells during experimental human influenza

Suzanna Paterson[1‡], Satwik Kar[1‡], Seng Kuong Ung[1], Zoe Gardener[1], Emma Bergstrom[1], Stephanie Ascough[1], Mohini Kalyan[1], Joanna Zyla[2,6], Jeroen Maertzdorf[2], Hans-Joachim Mollenkopf[2], January Weiner[2], Agnieszka Jozwik[3], Hannah Jarvis[3], Akhilesh Jha[3], Bradly P. Nicholson[4], Timothy Veldman[5], Chris W. Woods[5], Patrick Mallia[3], Onn Min Kon[3], Stefan H.E. Kaufmann[2], Peter J. Openshaw[3] & Christopher Chiu[1]*.

[1]Department of Infectious Disease, Imperial College London, Hammersmith Campus, Du Cane Road, London W12 0NN, United Kingdom.

[2]Max Planck Institute for Infection Biology, Berlin, Germany.

[3]National Heart and Lung Institute, Imperial College London, St Mary's Campus, London W2 1PG, United Kingdom.

[4]Durham Veteran's Affairs Medical Center, Durham, NC 27705, USA.

[5]Center for Applied Genomics and Precision Medicine, Department of Medicine, Duke University, Durham, NC 27708, USA.

[6]Department of Data Science and Engineering, Silesian University of Technology, Poland

[‡]These authors contributed equally.

*Corresponding author

Author contributions: CC, PJO, SHEK, CWW and TV designed the work. SP, SK, SKU, ZG, EB, SA, MK, AJ, HJ, AJ, BPN, PM, OMN and CC acquired data. SP, SK, JZ, JM, HJM, JW, AJ, PJO and CC analysed and interpreted the data. SP, SK and CC drafted the work. All authors reviewed, revised and approved the final version.

Sources of support: This work was supported by the European Commission's Seventh Framework Programme PREPARE (grant HEALTH-F3-2013-602525) and Biomarkers for

enhanced Vaccines immunoSafety (BioVacSafe) Innovative Medicines Initiative Grants; the Kwok Foundation; and DARPA Prometheus programme. PO and CC are supported by the Biomedical Research Centre (BRC) award to Imperial College Healthcare NHS Trust. Infrastructure support was provided by the NIHR Imperial Biomedical Research Centre and the NIHR Imperial Clinical Research Facility. The views expressed are those of the author(s) and not necessarily those of the NHS, the NIHR or the Department of Health and Social Care.

Short running head: Human lung-resident CD8+ T cells during influenza

Descriptor: 7.18

Word count (manuscript): 3715

This article has an online data supplement, which is accessible from this issue's table of content online at www.atsjournals.org

Abstract

Rationale: Suboptimal vaccine immunogenicity and antigenic mismatch, compounded by poor uptake, means that influenza remains a major global disease. T-cells recognising peptides derived from conserved viral proteins could enhance vaccine-induced cross-strain protection.

Objectives: To investigate the kinetics, phenotypes and function of influenza virus-specific CD8+ resident-memory T-cells (Trm) in the lower airway and infer the molecular pathways associated with their response to infection *in vivo*.

Methods: Healthy volunteers, aged 18-55, were inoculated intranasally with influenza A(H1N1)2009. Blood, upper and (in a subgroup) lower airway samples were obtained throughout infection. Symptoms were assessed using self-reported diaries and nasal viral load by qPCR. T-cell responses were analysed by three-colour FluoroSpot, flow cytometry with MHC I-peptide tetramers and RNAseq, with candidate markers confirmed using immunohistochemistry of endobronchial biopsies.

Measurements and Main Results: Following challenge, 57% of participants became infected. Pre-existing influenza-specific CD8+ T-cells in blood correlated strongly with reduced viral load, which peaked at day 3. Influenza-specific CD8+ T-cells in BAL were highly enriched and predominantly expressed the Trm markers CD69 and CD103. Comparison between pre-infection CD8+ T-cells in BAL and blood by RNAseq revealed 3928 differentially expressed genes, including all major Trm cell markers. However, gene-set enrichment analysis of BAL CD8+ T-cells showed primarily innate cell-related pathways and, during infection, included upregulation of innate chemokines (*Cxcl1*, *Cxcl10* and *Cxcl16*) that were also expressed by CD8+ cells in bronchial tissues.

Conclusions: CD8+ Trm cells in the human lung display innate-like gene and protein expression that demonstrates blurred divisions between innate and adaptive immunity.

Word count: 249

Key words: Influenza, CD8+ T-cell, resident memory, controlled human infection

Introduction

Despite vaccines, influenza remains one of the most important causes of severe infection worldwide[1]. Even with annual re-engineering to cover circulating strain mutation[2], vaccine effectiveness is often poor due to suboptimal immunogenicity and antigenic mismatch[3,4]. Seasonal influenza therefore still affects 10-46% of the global population each year, with mortality of 290-650,000 per annum[1], increasing during pandemics.

Since T-cells recognise peptides derived from conserved viral proteins, they can confer cross-strain protection[5]. However, systemic T-cell-inducing vaccines have shown limited efficacy. This may be due to the tissue-restricted nature of most respiratory viral disease and the need for antiviral effectors to act rapidly at the site of infection. In this context, circulating T-cells may represent surrogates rather than correlates of protection (surrogates being statistically associated but not mechanistically responsible for protection while correlates of protection are both)[6]. Resident memory T (Trm) cells are a tissue-restricted memory subset, poised at sites of potential infection to prevent disease through rapid responses to antigen re-exposure[6]. In murine influenza models, they offer greater heterosubtypic protection than patrolling central memory CD8+ T-cells of the same specificity[7]. However, the essential determinants of Trm cell generation and maintenance in humans remain unclear. Furthermore, unlike Trm cells at other anatomical sites, pulmonary Trm cells do not persist due to attrition and relocation to draining lymph nodes[8]. Maintaining them at the site of infection may therefore require specific local signals[9,10]. Recent studies have shown that local amplification can occur by *in situ* proliferation after secondary infection[11] or by recruitment of specialised memory cells that preferentially re-establish tissue residency[12]. Mucosal vaccine delivery could therefore optimise these responses in the human respiratory tract[10,13].

In humans, almost all published work on lung Trm cells has used resected tissue *post mortem* or *ex vivo*[14,15]. To investigate human virus-specific CD8+ T-cells *in vivo*, we previously challenged volunteers with respiratory syncytial virus (RSV) and revealed the correlation

between lower airway Trm cells and reduced disease severity[16]. Here, we have experimentally infected individuals with influenza A(H1N1)2009 virus to further investigate the differentiation of pulmonary CD8+ Trm cells. Using MHC class I-peptide tetramers, RNA sequencing and confocal microscopy, we identify influenza-specific CD8+ T-cell responses in the lower airways and demonstrate the molecular pathways associated with human Trm cells during *in vivo* infection. Some of the results of these studies have been previously reported in the form of abstracts.[17,18]

Materials and Methods

Study Design

Healthy adults (18-55 years) with haemagglutination inhibition (HAI) titre ≤1:10 against influenza A/California/04/2009 were enrolled. Clinical sampling and sample processing was undertaken as previously described[19]. The study was approved by the UK Research Ethics Service (reference 11/LO/1826).

Viral Load

Quantitative PCR was performed on nasal lavage samples as previously described[19], using pan-IAV M gene primers and probes (forward: GACCRATCCTGTCACCTCTGAC, reverse: AGGGCATTYTGGACAAAKCGTCTA, probe: TGCAGTCCTCGCTCACTGGGCACG)[19].

Fluorospot

Human IFN-γ/IL-2/TNF Fluorospot kits (Mabtech) were used according to the manufacturer's instructions to analyse cryopreserved PBMCs with pooled 9-mers representing conserved immunodominant MHC class I peptide epitopes (BEI Resources). Spots were read using AID ELISPOT 3.1.1 HR software (Autoimmune Diagnostika).

Immunohistochemistry and Confocal Microscopy

Endobronchial tissue biopsies were processed as previously described[19]. Four-micron thick microtome sections were co-stained using anti-CD8 antibody and anti-influenza (NP), anti-CD14, anti-Viperin, anti-MIP3-α, anti-CXCR1, anti-CXCL16, anti-IP10, anti-FABP4, anti-BAFF, anti-CD69 and CD103 (all Abcam, Supplementary Table 2). An HCF1-Zeiss LSM-780 inverted microscope was used for visualisation and Fiji Software for analysis.

Flow Cytometry

Whole blood and BAL cells were stained using HLA Class I (A*01:01-CTELKLSDY [#TS-M045-2] and A*02:01-GILGFVFTL [#TB-0012-M2]) tetramers (MBL International, Woburn, USA) as previously described[19]. Antibodies for phenotypic analysis are listed in Supplementary Table 2 and analysis was with FlowJo software (FlowJo LLC, USA). Cell sorting was achieved using a BD FACS Aria II sorter (BD Biosciences).

RNA Sequencing

RNA sequencing was performed on an Illumina HiSeq1500, with reads aligned using STAR and quality control using FastQC[20,21]. Further analysis was performed using edgeR, glmFit was and tmod R packages.[22–24] Data were deposited in the NCBI's Gene Expression Omnibus (accession number GSE175551).

Statistical Analysis

Statistical analysis was performed using Graphpad Prism and R software. Two-group comparisons were tested using Mann-Whitney test for unpaired and Wilcoxon matched-pairs signed rank test for paired groups. Multiple group comparisons were made using Friedman test with post-hoc Dunn tests.

Results

Influenza viral load correlates with symptom severity in experimentally infected adults

Forty-two participants with haemagglutination inhibition titres ≤1:10 were enrolled (Figure 1a & 1b). Fourteen of the 42 individuals additionally underwent up to three bronchoscopies (at pre-inoculation, day 7 and day 28 post-inoculation). Following inoculation, 24 participants (57.1%) developed symptomatic PCR-confirmed infection. There were no significant demographic differences between infected and uninfected individuals (Table 1). Median viral load peaked three days post-infection, at 3.33 (range 0 – 5.63) log10 copies/ml. No virus was detected beyond day 9 post-inoculation (Figure 1c). Of the 6 infected individuals who underwent bronchoscopies 2 had a detectable viral load on Day 7 bronchoscopy. Symptoms (primarily upper respiratory) began 24 hours post-infection and peaked around day 5 (Figure 1d and 1e). Eleven infected individuals (45.8%) had a temperature of >37.9°C at least once. Thus, experimental influenza A(H1N1)2009 infection caused a range of clinical outcomes despite uniformly low pre-inoculation HAI antibody levels.

Circulating memory CD8+ T-cells correlate with reduced influenza disease

The contribution of CD4+ and CD8+ T-cells as correlates of protection against influenza disease has varied depending on study design and virus strain[25,26]. To test the association of circulating CD8+ T-cells with protection against influenza A(H1N1)2009, PBMCs from 39 participants were assessed by Fluorospot with pooled conserved CD8+ T-cell epitopes. Prior to infection, influenza-specific T-cells could be quantified in almost all participants, albeit at modest frequencies (median 28 spots per million PBMCs, 5-74 range)(Figure 2a). There was no difference in influenza-specific T-cell frequencies between those who resisted infection and those who succumbed (p=0.9373). However, the frequency of pre-existing influenza-specific CD8+ T-cells correlated strongly with reduced viral load on subsequent infection (Spearman's rs=-0.7918, p=0.0007)(Figure 2b) and a similar trend was seen with symptom scores (Supplementary Figure 1a).

In 12 participants, cell numbers allowed analysis of complete time-courses and the breadth of CD8+ T-cell responses was analysed. CD8+ T-cells expanded significantly in all infected

participants (p=0.0475, mean fold-change 7.68) (Figure 2c, Supplementary Figure 1b) but not those remaining uninfected. By day 28, these had contracted to leave a minimally enlarged memory pool (p=0.4703). Both size and breadth of responses were heterogeneous but M1-specific T-cells were the most consistently expanded. In some individuals PB1-, NS2- and M2-specific T-cell populations also contributed substantially to the total response.

Polyfunctional T-cells that express multiple cytokines or effector molecules are associated with greater antiviral efficacy[27]. Using 3-colour Fluorospot, the capacity of individual cells to co-express IFN-γ, TNF and IL-2 was therefore enumerated in infected individuals (Figure 2d & 2e, Supplementary Figure 2). Prior to infection, most influenza-specific CD8+ T-cells expressed a single cytokine but 40% were polyfunctional and expressed all three. At day 7, single cytokine-producing T-cells preferentially increased. However, by the convalescent time-point, these proportions had returned to baseline. Together, these data suggest that during acute infection, the expansion of M1-, PB1-, M2- and NS2-specific T-cells is mainly made up of single cytokine-secreting cells, which disappear once infection resolves.

Influenza-specific CD8+ T-cells are enriched in the respiratory tract throughout infection

Circulating influenza-specific memory T-cells may represent surrogates rather than correlates of protection, with direct effector mechanisms more likely to act in the respiratory tract. Seven days post-inoculation, the bronchial mucosa of the 5 infected individuals showed macroscopic inflammation with erythema and micro-haemorrhages that resolved by day 28 (Figure 3a). Concurrently, CD8+ T-cells analysed by flow cytometry in the blood of 9 and BAL of 4 participants, showed transient upregulation of CD38 and Ki-67 (markers of activation and proliferation, respectively) in both blood (p=0.0002) and BAL (p=0.0286) at day 7 (Figure 3b & 3c). At this time-point, the frequency of activated CD8+ T-cells was also significantly higher in BAL than blood (p=0.0101).

MHC-peptide tetramers were then used to track epitope-specific cells in participants with suitable HLA types. In blood, tetramer+CD8+ T-cells underwent classical proliferation followed by contraction (Figure 3d & 3e). This was paralleled by BAL tetramer+ populations that showed a similar pattern of proliferation between day 0 and day 7 (p=0.0286) although approximately 5-fold higher in frequency (p=0.0112)(Figure 3f & 3g).

Trafficking of activated influenza-specific CD8+ T-cells alters subset composition in BAL

Epitope-specific CD8+ T-cells also upregulated Ki-67 and CD38 at day 7 post-infection (p=0.0039)(Figure 4a, Supplementary Figure 3a), with a similar pattern in BAL. CD8+ Trm cells are recognised by expression of CD69 and CD103 but in blood, few influenza-specific CD8+ T-cells expressed these markers, despite their recognised roles as activation markers (Figure 4b). In contrast, although tetramer+ CD8+ T-cells were only present at low frequencies in BAL pre-infection, almost all co-expressed CD69 and CD103. Following infection, the expanded tetramer+ population became comprised of both CD69+CD103+ and CD69 single-positive sub-populations. A CD69 single-positive cell population was not however seen in blood, implying that it was up-regulated only within the lung or airway. During convalescence, a trend towards increased CD103 co-expression then suggested progressive differentiation to the full Trm phenotype.

Blood and BAL CD8+ T-cells also differed markedly in terms of subset composition, with almost no naïve T-cells in BAL at any time-point (Figure 4c). With infection, influenza-specific CD8+ T-cells in both blood and BAL primarily displayed an effector/effector memory phenotype. This altered balance of T-cell subsets persisted to day 28 despite proliferation having ceased. In blood, the change in subset composition was also reflected in the co-stimulatory molecules CD27 and CD28 (Figure 4d), with high expression of both markers at day 7 followed by downregulation of CD27 by day 28. In contrast, the majority of BAL CD8+ Trm cells did not express CD27 and CD28 at rest but became predominantly double-positive during infection (median 65.6% IQR 81.1-46.5%) before being rapidly downregulated. This

was paralleled by the expression of cytotoxicity markers perforin and granzyme B in BAL cells, with the majority (median 52.0% IQR 58.7-50.8%) significantly upregulating these markers at day 7 but almost no expression at day 28 (Figure 4e).

Finally, activation was associated with upregulation of the chemokine receptors CCR5 and CXCR3, promoting chemotaxis to inflamed tissues and the lung respectively. In blood, 50% (IQR 62.9-7.15) of influenza-specific CD8+ T-cells expressed both receptors at rest, increasing to 97.8% (IQR 99.5-92.4%) during infection (Figure 4f). In BAL, even resting influenza-specific Trm cells were mostly CCR5+CXCR3+ (median 71.4% IQR 77.8-50%) which further increased to 94.5% (IQR 98.88-66.28%) at day 7. These data therefore show distinct phenotypic changes that occur between BAL and blood, supporting pre-clinical data of acutely activated influenza-specific CD8+ T-cells that home to the lung via chemokine receptors.

Transcriptomic signatures of compartmentalisation in human BAL and blood CD8+ T-cells

The molecular determinants of Trm cell generation in humans are poorly understood, so CD8+ T-cells were sorted from blood and BAL of 12 individuals for analysis by RNA sequencing (Supplementary Figure 3b & 3c). Due to limited BAL cell numbers, bulk CD45+CD14-CD19-CD3+CD8+ cells were analysed. All sorts were at least 95% pure with any remaining non-CD8+ cells negative for other leukocyte markers CD45, CD14 and CD19 (Supplementary Figure 3b).

Differential gene expression comparing blood and BAL CD8+ T-cells pre-infection revealed 4,699 differentially expressed genes (DEGs, FDR<0.05, Supplementary Table 3). However, since immunophenotyping had shown the markedly different composition of CD8+ T-cells from these two compartments (Figure 4), some genes were likely to have represented only differences between naïve and memory T-cells. To enrich the DEG list for genes specifically associated with Trm cells in the lung, DEGs from two previous studies[28,29] that distinguished

naïve from memory T-cells were therefore excluded. This resulted in 3,928 DEGs for continued analysis (Figure 5a, Supplementary Table 4). Among the top 20% most significantly differentially expressed genes in this list, all major markers associated with Trm cells were present, including *CD69*, CD103 (*ITGAE*), CD49a (*ITGA1),* fatty acid binding protein 4 (*FABP4*), and *S1PR1* (down-regulated in BAL CD8+ T-cells) (Figure 5b & 5c). Additionally in the full gene list, 29 of the 31 genes previously proposed[30] as a core signature of Trm cells across different tissues were concordant (*CA10, ITGA1, ITGAE, IL2, IL10, CXCR6, CXCL13, KCNK5, RGS1, DUSP6, PDCD1, IL23R* [upregulated in Trm cells] and *STK38, TTC16, SELL, KLF2, KLF3, SBK1, TTYH2, NPDC1, KRT72, S1PR1, SOX13, KRT73, TSPAN18, PTGDS, RAP1GAP2, CX3CR1* [downregulated in Trm cells])(Figure 5b; Supplementary Table 3).

Next, to identify functional pathways, gene set enrichment analysis was performed using the CERNO algorithm[22]. Surprisingly, the most significantly enriched gene sets were not associated with known T-cell functions. Instead, the top gene set was annotated as “Enriched in monocytes” with 10/24 of the most significantly enriched gene sets labelled as monocyte, dendritic cell and other innate cell pathways (Figure 5d, Supplementary Table 5). Surprisingly, these included the myeloid cell marker and LPS receptor CD14 despite this having been used to dump non-T-cells for FACS sorting. The remaining pathways comprised generic cellular activities (cell cycle and transcription, endoplasmic reticulum, extracellular matrix) and common immune response pathways (including immune activation, Toll-Like Receptor [TLR] and inflammatory signalling and cytokine and chemokine-related pathways). Only one gene set (CD4 T-cell surface signature Th1-stimulated) was specifically T-cell-related.

Differential gene expression by CD8+ T-cells in BAL during influenza is dominated by innate-like signatures

Comparing the transcriptomes of CD8+ cells between blood and BAL is confounded by steady-state differences in subset composition. However, longitudinal analysis of cells from the same anatomical compartment removes the contribution of cells that remain unchanged

during infection. Comparing CD8+ T-cells in BAL at day 7 post-infection with pre-infection samples, 62 DEGs (FDR<0.05) were identified (Figure 5e). These included the activation marker CD38 and the co-stimulatory marker CD28, which were also upregulated at day 7 in our cytometry data (Figure 4). In contrast, only 25 DEGs were identified in blood at the same time-points (Supplementary Figure 5, Supplementary Tables 5 & 6).

Using the tmod R package, three major patterns of functional enrichment were revealed. Around half of the significantly enriched pathways up-regulated at day 7 post-infection were shared by both blood and BAL CD8+ cells (Figure 5f). These were primarily related to cell division or pattern recognition receptor and innate interferon signalling. The second pattern involved up-regulation only in BAL CD8+ cells at day 7 post-infection. These partly recapitulated the findings in resting BAL CD8+ T-cells, with up-regulated pathways predominantly relating to monocytes and dendritic cells, as well as cell cycle and effector functions such as lysosomal/endosomal pathways (Supplementary Table 7). Finally, a smaller set of pathways was uniquely enriched only in blood CD8+ cells, again related to cellular proliferation, plus DNA repair and RIG-I signalling. By day 28, these changes had largely resolved in both blood and BAL (Supplementary Table 8 & 9). No MAIT or NKT cell modules were found to be enriched.

CD8+ T-cells infiltrating the bronchial mucosa during influenza infection express innate-like markers

To identify CD8+ Trm cells infiltrating the bronchial mucosa, endobronchial biopsies were co-stained with anti-CD8, CD69 and CD103 (Figure 6a-6d). At the acute time-point, CD8+ cells were abundant in both epithelium and subepithelium despite no detectable staining for influenza virus antigen (Figure 6a & 6b, Supplementary Figure 6a). CD69 was co-expressed in 39% of CD8+ cells with strong co-localisation (correlation coefficient 0.79), while CD103 was co-expressed in 78% (correlation coefficient 0.58)(Figure 6e & 6f). Co-expression of CD69 and CD103 was observed in 36% of CD8+ cells, similar to that seen in BAL CD8+ Trm

cells quantified by flow cytometry (Figure 4b). Additionally, FABP4 was co-expressed on 30% of CD8+ cells (correlation coefficient 0.64, Supplementary Figure 6b).

To confirm the unexpected finding of innate-like gene expression in BAL CD8+ T-cells, bronchial tissue was stained for selected markers representative of the most statistically enriched pathways. The topmost significant DEGs contributing to the myeloid cell and viral sensing pathways were selected to validate genes not typically associated with CD8+ T-cells. *CD14* was the most significantly differentially expressed gene in "Myeloid cell enriched receptors and transporters" (Figure 6g); *TNFSF13B* (or BAFF) in "Viral sensing and immunity: IRF2 targets network" (Supplementary Figure 6c); *RSAD2* (Viperin) in "Enriched in activated dendritic cells" (Supplementary Figure 6d); *CXCL1* in "Enriched in activated dendritic cells" (Figure 6h) *CXCL10* fourth highest in "Viral sensing and immunity: *IRF2* targets network (II)" (Figure 6i); *CXCL16* second highest in "DC surface signature" (Figure 6j); and *CCL20* (MIP-3b) in "Enriched in activated dendritic cells" (Supplementary Figure 6e). For these markers, co-expression was observed in 32-94% of CD8+ cells at day 7 post-infection with correlation coefficients of 0.74-0.97, indicating that all markers were strongly correlated with CD8 in co-expressed cells (Figure 6e & 6f).

Thus, we identified distinctive innate-like patterns of gene expression by human BAL CD8+ T-cells responding to influenza infection *in vivo*, consistent with the rapid innate-like effector functions that Trm cells possess.

Discussion

In this study, we tracked CD8+ Trm cells in adults challenged with influenza A(H1N1)2009 *in vivo*. Pre-existing circulating memory CD8+ T-cells correlated strongly with reduced viral load (in support of previous studies[25,31,26]) and were temporally associated with virus-specific counterparts in the lung. However, antigen-specific CD8+ T-cells in blood and airway displayed markedly divergent kinetics, phenotype and functional characteristics, with airway

CD8+ cells unexpectedly dominated by transcriptomic signatures usually associated with innate immune cells. This suggests that while peripheral blood memory T-cells may be strong surrogates of protection, they poorly represent Trm cells that act most directly to eliminate virus.

Despite correlations between circulating memory T-cells and reduced disease, systemic T-cell-inducing vaccines are yet to demonstrate substantial efficacy. We propose that this is due to differences in tissue localisation of T-cells generated after infection and systemic vaccination[32]. In murine influenza, Trm cells prevent lethal infection better than their systemic counterparts and are sufficient to confer cross-strain immunity[7]. Pulmonary Trm cell generation requires not only antigen, but also co-stimulation and signals from the microenvironment for differentiation and tuning of responses[33]. Importantly, these signals are tissue-restricted and require local monocytes and dendritic cells[34]. This is supported by our data, which show influenza-specific CD69+CD103-CD8+ T-cell appearing in bronchial mucosa and BAL but not blood during acute infection with increased acquisition of the CD69+CD103+ phenotype into convalescence, implying local upregulation of CD69 and later CD103. However, even with these signals, murine lung-resident Trm cells wane over time, caused by redistribution and imbalance between apoptosis and replenishment in the amino acid-poor lung environment[10,35]. In humans, lung transplant data suggests that both *in situ* Trm cell maintenance and *de novo* recruitment can occur[36]. Furthermore, some Trm cells may re-enter the circulation after resolution but preferentially return on repeat infection enabling more rapid recall on local re-stimulation, that suggests a role for mucosal vaccination to enhance these responses[12].

One previous study using post-mortem tissues identified a core transcriptional signature common to Trm cells from multiple sites[30]. While that study sorted T-cells on the basis of CD69 expression, the limited cell numbers obtained from *in vivo* BAL meant that this was not possible here. Therefore, a proportion of the DEGs we identified between blood and BAL

CD8+ cells are likely to have represented differences in subset composition. Nevertheless, 94% of the genes in the earlier core profile were identified. However, the most significantly enriched pathways were functionally annotated as monocyte- and dendritic cell-related, despite no evidence of contamination by myeloid cells.

Classical T-cells make up by far the largest proportion of CD3+CD8+ cells in the lung, though non-classical CD8-expressing T-cells are also present. These include MAIT-cells, iNKT-cells and γδ T-cells, all of which have subpopulations expressing CD8. MAIT-cells make up around 2% of CD3+ cells in both blood and BAL of healthy adults, so in numerical terms these cells are unlikely to contribute substantially to differential gene expression. Similarly, invariant NKT-cells are rare in humans, ranging in frequency between 0.1 and 1% in peripheral blood and are mostly CD8-. In mice they are mainly localised in the pulmonary vasculature and interstitium[37]. Although γδ T-cells make up 8-20% of pulmonary lymphocytes in mice, the majority are CD4-CD8- double negative[38]. Nevertheless, to mitigate the contribution of unconventional T-cells, we undertook longitudinal analysis, controlling for systematic differences in CD8+ subset composition. Furthermore, these signatures were unlikely to have been due to innate cells at the day 7 timepoint, since most (including MAIT-cells) normally respond more immediately and to lower peak abundance, although this remains to be definitively shown using single-cell techniques[39].

We therefore conclude that CD8+ Trm cells in the airway express innate-like features that underlie their sentinel function. These pathways included Pathogen Associated Molecular Patterns recognition by TLRs, implied by the upregulation of CD14 detected in CD8+ cells in bronchial biopsies. We hypothesise CD14 here to be intracellular and therefore only revealed following detergent antigen retrieval for confocal microscopy. TLR4 and CD14 have previously been implicated in RSV and IAV recognition by alveolar macrophages, with CD14 observed on CD8+ T-cells during HIV infection, in severe asthma, and after *in vitro* stimulation allowing direct recognition of LPS[40,41]. Downstream signalling regulates expression of pro-

inflammatory and interferon-stimulated genes (ISGs), including viperin, which has antiviral activity and is involved in regulation of CD4+ T-cell responses[42,43]. In addition, our data suggest that CD8+ Trm cell activation is associated with the production of innate mediators, including B-cell activation factor (BAFF) which has a role in T-cell co-stimulation[44] and the chemokines CXCL1, CXCL10, CXCL16 and CCL20 (which are all commonly expressed by myeloid cells but, in the case of CXCL10 and CXCL16, have also been reported in T-cells). Together, we hypothesise that these function to enhance chemoattraction, rapidly reinforcing the antiviral inflammatory environment[45,46].

The major limitation of this study is the small number of infected participants who underwent lower airway sampling, which led to further restrictions on sample size once HLA matching to enable tetramer-labelled lower airway T cell analysis was undertaken. Nevertheless, differences in these cells were sufficiently consistent for us to show that human pulmonary CD8+ memory T cells share phenotypic and transcriptional characteristics with other immune cells that act immediately when pathogens are encountered. These findings parallel recent transcriptomic studies of pulmonary CD8+ Trm cells in mice, which also upregulate cell cycle genes, macrophage-associated chemokines (such as CCL3, CCL9 and CXCL10) and interferon-stimulated genes[47]. We therefore propose that these are essential features of the CD8+ Trm cell response that may be targeted through adjuvantation (e.g. by direct signalling through the TLR4 pathway[41]) and indicate the blurred distinction between innate and adaptive immunity in this setting.

References

1. WHO. Influenza (Seasonal). https://www.who.int/news-room/fact-sheets/detail/influenza-(seasonal). Accessed 20/05/2020.
2. Krammer, F. & Palese, P. Advances in the development of influenza virus vaccines. *Nat. Rev. Drug Discov.* **14**, 167–182 (2015).

3. Cobey, S. *et al.* Poor immunogenicity, not vaccine strain egg adaptation, may explain the low H3N2 influenza vaccine effectiveness in 2012-13. *Clin. Infect. Dis. Off. Publ. Infect. Dis. Soc. Am.* (2018) doi:10.1093/cid/ciy097.
4. Pebody, R. *et al.* Low effectiveness of seasonal influenza vaccine in preventing laboratory-confirmed influenza in primary care in the United Kingdom: 2014/15 mid-season results. *Euro Surveill. Bull. Eur. Sur Mal. Transm. Eur. Commun. Dis. Bull.* **20**, (2015).
5. Koutsakos, M. *et al.* Human CD8 + T cell cross-reactivity across influenza A, B and C viruses. *Nat. Immunol.* **20**, 613–625 (2019).
6. Schenkel, J. M. & Masopust, D. Tissue-Resident Memory T Cells. *Immunity* **41**, 886–897 (2014).
7. Wu, T. *et al.* Lung-resident memory CD8 T cells (TRM) are indispensable for optimal cross-protection against pulmonary virus infection. *J. Leukoc. Biol.* **95**, 215–224 (2014).
8. Stolley, J. M. *et al.* Retrograde migration supplies resident memory T cells to lung-draining LN after influenza infection. *J. Exp. Med.* **217**, (2020).
9. Van Braeckel-Budimir, N., Varga, S. M., Badovinac, V. P. & Harty, J. T. Repeated Antigen Exposure Extends the Durability of Influenza-Specific Lung-Resident Memory CD8+ T Cells and Heterosubtypic Immunity. *Cell Rep.* **24**, 3374-3382.e3 (2018).
10. Slütter, B. *et al.* Dynamics of influenza-induced lung-resident memory T cells underlie waning heterosubtypic immunity. *Sci. Immunol.* **2**, eaag2031 (2017).
11. Park, S. L. *et al.* Local proliferation maintains a stable pool of tissue-resident memory T cells after antiviral recall responses. *Nat. Immunol.* **19**, 183–191 (2018).
12. Fonseca, R. *et al.* Developmental plasticity allows outside-in immune responses by resident memory T cells. *Nat. Immunol.* **21**, 412–421 (2020).

13. Mackay, L. K. *et al.* Long-lived epithelial immunity by tissue-resident memory T (TRM) cells in the absence of persisting local antigen presentation. *Proc. Natl. Acad. Sci.* **109**, 7037–7042 (2012).
14. Sathaliyawala, T. *et al.* Distribution and compartmentalization of human circulating and tissue-resident memory T cell subsets. *Immunity* **38**, 187–197 (2013).
15. de Bree, G. J. *et al.* Selective accumulation of differentiated CD8+ T cells specific for respiratory viruses in the human lung. *J. Exp. Med.* **202**, 1433–1442 (2005).
16. Jozwik, A. *et al.* RSV-specific airway resident memory CD8+ T cells and differential disease severity after experimental human infection. *Nat. Commun.* **6**, 10224 (2015).
17. Paterson, S. Innate-like signatures of influenza-specific CD8+ T cell responses in the human lung. *OPTIONS X Control Influenza* (2019).
18. Kar, Satwik. Dynamic signatures of human lung resident memory CD8+ T cells during experimental influenza infection. in (2018).
19. Jozwik, A. *et al.* RSV-specific airway resident memory CD8+ T cells and differential disease severity after experimental human infection. *Nat. Commun.* **6**, (2015).
20. Dobin, A. *et al.* STAR: ultrafast universal RNA-seq aligner. *Bioinformatics* **29**, 15–21 (2013).
21. Wingett, S. W. & Andrews, S. FastQ Screen: A tool for multi-genome mapping and quality control. *F1000Research* **7**, (2018).
22. Zyla, J. *et al.* Gene set enrichment for reproducible science: comparison of CERNO and eight other algorithms. *Bioinformatics* **35**, 5146–5154 (2019).
23. Li, S. *et al.* Molecular signatures of antibody responses derived from a systems biological study of 5 human vaccines. *Nat. Immunol.* **15**, 195–204 (2014).
24. Chaussabel, D. *et al.* A modular analysis framework for blood genomics studies: application to systemic lupus erythematosus. *Immunity* **29**, 150–164 (2008).

25. Wilkinson, T. M. *et al.* Preexisting influenza-specific CD4+ T cells correlate with disease protection against influenza challenge in humans. *Nat. Med.* **18**, 274–280 (2012).
26. Sridhar, S. *et al.* Cellular immune correlates of protection against symptomatic pandemic influenza. *Nat. Med.* **19**, 1305–1312 (2013).
27. Lin, L. *et al.* COMPASS identifies T-cell subsets correlated with clinical outcomes. *Nat. Biotechnol.* **33**, 610–616 (2015).
28. Akondy, R. S. *et al.* Origin and differentiation of human memory CD8 T cells after vaccination. *Nature* **552**, 362–367 (2017).
29. Kaech, S. M., Hemby, S., Kersh, E. & Ahmed, R. Molecular and functional profiling of memory CD8 T cell differentiation. *Cell* **111**, 837–51 (2002).
30. Kumar, B. V. *et al.* Human Tissue-Resident Memory T Cells Are Defined by Core Transcriptional and Functional Signatures in Lymphoid and Mucosal Sites. *Cell Rep.* **20**, 2921–2934 (2017).
31. McMichael, A. J., Gotch, F. M., Noble, G. R. & Beare, P. A. Cytotoxic T-cell immunity to influenza. *N Engl J Med* **309**, 13–7 (1983).
32. Liu, Y., Ma, C. & Zhang, N. Tissue-specific Control of Tissue Resident Memory T Cells. *Crit. Rev. Immunol.* **38**, 79–103 (2018).
33. Szabo, P. A., Miron, M. & Farber, D. L. Location, location, location: Tissue resident memory T cells in mice and humans. *Sci. Immunol.* **4**, eaas9673 (2019).
34. Dunbar, P. R. *et al.* Pulmonary monocytes interact with effector T cells in the lung tissue to drive T RM differentiation following viral infection. *Mucosal Immunol.* **13**, 161–171 (2020).
35. McMaster, S. R. *et al.* Pulmonary antigen encounter regulates the establishment of tissue-resident CD8 memory T cells in the lung airways and parenchyma. *Mucosal Immunol.* **11**, 1071–1078 (2018).

36. Snyder, M. E. *et al.* Generation and persistence of human tissue-resident memory T cells in lung transplantation. *Sci. Immunol.* **4**, eaav5581 (2019).

37. Hinks, T. S. C. *et al.* Innate and adaptive T cells in asthmatic patients: Relationship to severity and disease mechanisms. *J. Allergy Clin. Immunol.* **136**, 323–333 (2015).

38. Kalyan, S. & Kabelitz, D. Defining the nature of human γδ T cells: a biographical sketch of the highly empathetic. *Cell. Mol. Immunol.* **10**, 21–29 (2013).

39. van Wilgenburg, B. *et al.* MAIT cells contribute to protection against lethal influenza infection in vivo. *Nat. Commun.* **9**, 4706 (2018).

40. Turner, D. *et al.* Overexpression of a Novel Lymphocyte Population, Positive for an Intracellular CD14-Like Antigen, in Patients Positive for Human Immunodeficiency Virus Type 1. *Clin. Diagn. Lab. Immunol.* **11**, 1040–1044 (2004).

41. Komai-Koma, M., Gilchrist, D. S. & Xu, D. Direct recognition of LPS by human but not murine CD8+ T cells via TLR4 complex. *Eur. J. Immunol.* **39**, 1564–1572 (2009).

42. Wang, X., Hinson, E. R. & Cresswell, P. The Interferon-Inducible Protein Viperin Inhibits Influenza Virus Release by Perturbing Lipid Rafts. *Cell Host Microbe* **2**, 96–105 (2007).

43. Qiu, L.-Q., Cresswell, P. & Chin, K.-C. Viperin is required for optimal Th2 responses and T-cell receptor–mediated activation of NF-κB and AP-1. *Blood* **113**, 3520–3529 (2009).

44. Hu, S. *et al.* BAFF promotes T cell activation through the BAFF-BAFF-R-PI3K-Akt signaling pathway. *Biomed. Pharmacother.* **114**, 108796 (2019).

45. Peperzak, V. *et al.* CD8 $^{+}$ T Cells Produce the Chemokine CXCL10 in Response to CD27/CD70 Costimulation To Promote Generation of the CD8 $^{+}$ Effector T Cell Pool. *J. Immunol.* **191**, 3025–3036 (2013).

46. Shashkin, P., Simpson, D., Mishin, V., Chesnutt, B. & Ley, K. Expression of CXCL16 in Human T Cells. *Arterioscler. Thromb. Vasc. Biol.* **23**, 148–149 (2003).

47. Low, J. S. *et al.* Tissue-resident memory T cell reactivation by diverse antigen-presenting cells imparts distinct functional responses. *J. Exp. Med.* **217**, e20192291 (2020).

Figure Legends

Figure 1: Experimental human infection with influenza A(H1N1)2009 virus induces a diversity of clinical outcomes. (a) Forty-two healthy adult volunteers were intranasally inoculated with influenza A(H1N1)2009 and sampled periodically post-inoculation. CONSORT diagram is shown. (b) Schematic showing schedule of sampling. (c) Viral load of 42 individuals as determined by M gene RT-PCR from nasal lavage. Individual data points and the mean (red) viral load are shown. (d) Self-reported total daily symptom scores for infected (red, n=23) and uninfected (blue, n=18) individuals. Data are shown as mean +/-s.e.m. (e) Upper respiratory tract (blue), lower respiratory tract (red) and systemic (green) symptom scores in infected participants. Data are shown as the mean +/-s.e.m. (e) Spearman's correlation analysis between viral load and symptom scores in infected individuals.

Figure 2: Circulating memory CD8+ T-cells correlate strongly with reduced disease severity in influenza. Influenza-specific CD8+ T-cells were quantified in blood by FluoroSpot following stimulation with conserved MHC class I epitopes. (a) Where cell numbers allowed, IFN-γ secreting influenza-specific T-cells were measured in PBMCs prior to inoculation obtained from participants who subsequently became infected (n=16) or remained uninfected (n=23). (b) Spearman's correlation between pre-inoculation influenza-specific T-cells and viral load in subsequently PCR+ individuals (n=16). rs=Spearman's rank correlation coefficient (c) Frequency of IFN-γ secreting T-cells stimulated with influenza peptides derived from internal influenza proteins at pre-infection, day 7 and day 28 timepoints. T-cell responses to conserved peptide derived from M1 and M2 (matrix); NA (neuraminidase); nucleoprotein (NP); non-structural protein 2 (NS2); and the RNA polymerase complex (PA, PB1 and PB2) are shown as median and IQR. (d) FluoroSpot images from one representative donor at day 7 post-infection are shown. (e) The proportion of T-cells secreting IFN-γ, TNFα, IL-2 or combinations of multiple cytokines in peptide-stimulated PBMCs is shown. Pie chart sections represent the proportion of cells with 1, 2 or 3 functions. Individual cytokines and their combinations are denoted by arcs.

Figure 3: Influenza-specific CD8+ T-cells are preferentially expanded in the human airway during experimental infection. Healthy adult volunteers were experimentally infected with IAV and serially sampled for blood and bronchoalveolar lavage (BAL). (a) Macroscopic appearances of the lower airway were assessed by bronchoscopy at pre-infection, day 7 and day 28. One representative individual is shown. (b) CD8+ T-cells in blood and BAL were co-stained with Ki-67 and CD38 for analysis by flow cytometry. P-values for Wilcoxon matched pairs tests for pairwise and Mann-Whitney tests for unpaired comparisons are shown (*$p<0.05$ and **$p<0.01$). (c) Flow cytometry plots are shown for one representative individual. (d) CD8+ T-cells labelled with A*01:01-CTELKLSDY or A*02:01-GILGFVFTL tetramer were quantified in blood. Individual data and median are shown. P-values for Friedman test with Dunn's multiple comparisons test are shown. (e) CD8+ T-cells in blood were labelled with A*02:01-GILGFVFTL tetramer. Flow cytometry plots are shown for one representative individual. (f) CD8+ T-cells labelled with A*01:01-CTELKLSDY or A*02:01-GILGFVFTL tetramer were quantified in BAL. Individual data and median are shown. (g) CD8+ T-cells in BAL were labelled with A*02:01-GILGFVFTL tetramer. Flow cytometry plots are shown for one representative individual. P-values for Wilcoxon matched pairs tests are shown (*$p<0.05$ and **$p<0.01$).

Figure 4: Influenza infection induces divergent phenotypic changes in blood and BAL. Whole blood/PBMCs (n=8) and BAL (n=4) from influenza-infected individuals were stained with tetramer, anti-CD3, CD4 and co-stained with (a) Ki-67 and CD38; (b) CD69 and CD103; (c) CD45RA and CCR7 (median and IQR are shown); (d) CD27 and CD28; (e) granzyme B and perforin; and (f) CCR5 and CXCR3 for analysis by flow cytometry. Median (red) and individual data are shown. P-values for Wilcoxon matched pairs tests are shown

for pair-wise comparisons of BAL cells and Friedman test with Dunn's multiple comparisons test for multiple comparisons of blood cells. (*p<0.05 and **p<0.01).

Figure 5: Resident memory CD8+ T-cells in the lower airway responding to influenza infection display innate-like signatures. Live CD3+CD4-CD14-CD19-CD8+ T-cells were sorted by FACS from blood and BAL of 12 individuals inoculated with IAV at pre-infection, day 7 and day 28 post-infection. (a) Diagrammatic representation of differential gene expression comparing compartments and timepoints. (b) Volcano plot showing differentially expressed genes in BAL vs blood CD8+ T-cells pre-infection. Red shows genes upregulated and blue genes downregulated in BAL. (c) Pre-infection expression levels of the Trm cell markers CD69, CD013, FABP4 and S1PR1 were compared between BAL and blood CD8+ T-cells. (d) Functionally annotated gene sets significantly enriched (log10 adjusted p value) with DEGs comparing BAL and blood CD8+ T-cells were identified using the tmod R package. Red line denotes the cut off for significance (FDR<0.05). (e) Volcano plot demonstrating significant DEGs in BAL CD8+ T cells from 5 infected individuals at day 7 post-infection compared with pre-infection. Significantly upregulated DEGs are highlighted in red, downregulated are in blue and significant DEGs are labelled with their gene symbols. (f) Functionally annotated gene sets significantly enriched with DEGs comparing CD8+ T-cells at each timepoint compared to its corresponding pre-infection timepoint in blood and BAL were identified using the tmod R package. All statistically significant DEGs without Bonferroni-Hochberg correction are included. The darker the red colouration the more significant the pathway enrichment.

Figure 6: CD8+ cells in the bronchial mucosa during influenza co-express Trm and innate-like markers. Endobronchial biopsies were obtained by bronchoscopy from healthy volunteers (n=9) inoculated with IAV. (a) Sections obtained from bronchial biopsies of PCR+ participants were stained with anti-CD8 and DAPI. Cells expressing CD8 (green) in the epithelial and sub-epithelial layers at baseline (left), day 7 with a magnified image at day 7, and day 28 (right) from one representative individual are shown. (b) Cells expressing CD8 were quantified in the mucosal epithelium and sub-epithelium in PCR+ (n=5) and PCR– (n=4) participants at pre-infection, day 7 and day 28 post-inoculation. (c) Sections were co-stained with anti-CD8 (FITC, green), anti-CD103 (Cy5, magenta), anti-CD69 (Cy3, red) and DAPI (blue) at day 7 post-infection. Representative images from one individual are shown. (d) Colocalization (yellow) of Trm markers (CD69 and CD103) with CD8 observed in the bronchial mucosa are represented in the magnified image. (e) The frequency of CD8+ cells expressing markers of tissue residence (CD69, CD103 and FABP4); stimulatory molecules (BAFF and CD14); interferon stimulated genes (viperin) and chemokines (CCL20, CXCL1, CXCL10 and CXCL16) was quantified in the mucosal epithelium (f) Co-localization correlation coefficients of each marker with CD8 in the mucosal epithelium was calculated. Biopsy sections (day 7) were co-stained with anti-CD8 (FITC, green) and (g) anti-CD14(Cy 5, Magenta); (h) anti-CXCL1 (Cy 5, Magenta) ; (i) anti-CXCL10 (Cy 5, Magenta) and (j) anti-CXCL16 (Cy 5, Magenta) with colocalization shown in yellow. One representative individual is shown. Data are representative of 3 independent experiments performed from biopsies obtained from 5 infected individuals (i.e. 5 biological replicates). Yellow arrows indicate cells with co-expression of CD8+ cells with other markers. Scale bars=20 μm.

Table 1: Study participant demographics. Demographic data summary of all subjects inoculated with influenza A(H1N1)2009 virus. Data shown compare individuals who underwent bronchoscopies with those who did not have bronchoscopies and all included individuals.

Supplementary Figure 1: Pre-existing influenza-specific T-cells in blood and symptom AUC. Influenza-specific CD8+ T-cells producing IFN-γ were quantified in blood by FluoroSpot following stimulation with conserved MHC class I epitopes. (a) Spearman's correlation between pre-inoculation influenza-specific T-cells and viral load in subsequently PCR+

individuals (n=16). rs=Spearman's rank correlation coefficient. (b) Individual data for infected and uninfected participants are shown.

Supplementary Figure 2: Cytokine production by influenza-specific T-cells in blood following infection. Influenza-specific CD8+ T-cells were quantified in blood by FluoroSpot following stimulation with conserved MHC class I epitopes and production of IFN-γ, TNF and IL-2 assessed.

Supplementary Figure 3: Phenotype and gating strategy for FACS analysis of CD8+ cells in blood and BAL. CD8+ T-cells were analysed by flow cytometry. (a) Heatmap shows the frequency of cells of each phenotype (green=0%, red=100%). (b) The gating strategy for analysis and FACS sorting is shown. (c) Post-sort analysis after sorting of blood and BAL for CD45+CD14-CD19-CD3+CD8+ cells.

Supplementary Figure 4: Venn diagram showing differentially expressed genes associated with naïve vs memory CD8+ T-cells excluded from further analysis.

Supplementary Figure 5: Volcano plot showing differentially expressed genes at day 7 vs day 0 post-infection in CD8+ cells from blood.

Supplementary Figure 6: Analysis of influenza antigen and innate marker expression in bronchial biopsy CD8+ cells by confocal microscopy. Endobronchial biopsies from PCR+ individual were stained with (a) anti-influenza (NP). No viral antigen was detected. Biopsy sections (day 7 post-infection) were co-stained with Anti-CD8 (FITC, green) and (b) anti-CCL20 (Cy 5, Magenta), (c) anti-BAFF (Cy5, Magenta), (d) anti-Viperin, (e) anti-FABP4. Co-localisation of CD8 with individual markers observed. Yellow arrows indicate cells with co-expression of CD8+ cells with other markers. Scale bars = 20 microns.

Supplementary Table 1: List of conserved CD8+ T-cells epitopes pooled for FluoroSpot analysis.

Supplementary Table 2: List of antibodies used for immunohistochemistry and confocal microscopy.

Supplementary Table 3: List of DEGs pre-infection between blood and BAL CD8+ T-cells. All individual gene descriptions, log fold change and adjusted p values are included. Gene functions are given for all genes with an adjusted p value of <0.05.

Supplementary Table 4: List of DEGs pre-infection between blood and BAL CD8+ T-cells (with DEGs associated with memory T cell differentiation removed). All individual gene descriptions, log fold change and adjusted p values are included. Gene functions are given for all genes with an adjusted p value of <0.05.

Supplementary Table 5: Pathway enrichment analysis pre-infection between blood and BAL CD8+ T-cells. All individual genes and gene descriptions within each module and their corresponding log fold change and p values are shown.

Supplementary Table 6: List of significant DEGs (FDR<0.05) at day 7, compared to pre-infection, in BAL CD8+ T-cells. All individual gene descriptions, log fold change and adjusted p values are included.

Supplementary Table 7: List of significant DEGs (FDR<0.05) at day 28, compared to pre-infection, in BAL CD8+ T-cells. All individual gene descriptions, log fold change and adjusted p values are included.

Supplementary Table 8: Gene set enrichment analysis at day 7 in BAL CD8+ T-cells. All individual genes and gene descriptions within each module and their corresponding log fold change and p values are shown.

Supplementary Table 9: List of significant DEGs (FDR<0.05) at day 28, compared to pre-infection, in blood CD8+ T-cells. All individual gene descriptions, log fold change and adjusted p values are included.

Table 1: Demographic characteristics of study participants

	Bronchoscopy		No Bronchoscopy		Overall	
Outcome	PCR +	PCR -	PCR +	PCR -	PCR +	PCR -
Number	5	9	19	9	24	18
Age in years (median & range)	51 (43-53)	53 (30-54)	35 (18-55)	40 (32-49)	42.5(18-55)	43 (30-54)
Sex (M:F)	2:3	8:1	14:5	6:3	16:8	14:4
Ethnicity						
White	3	6	9	8	6	14
Black British/black other	1	1	3	0	3	1
Asian British/Indian/Asian other	1	0	4	1	2	1
Mixed	0	0	2	0	2	0
Other	0	2	1	0	0	2
Median height (cm)	1.63	1.71	1.76	1.73	1.77	1.72
Median weight (kg)	66	82.6	73.5	75.5	73.2	76.75
Median BMI (kg m^{-2})	27.83	26.11	24.3	24.81	25.9	25.87

Figure 1

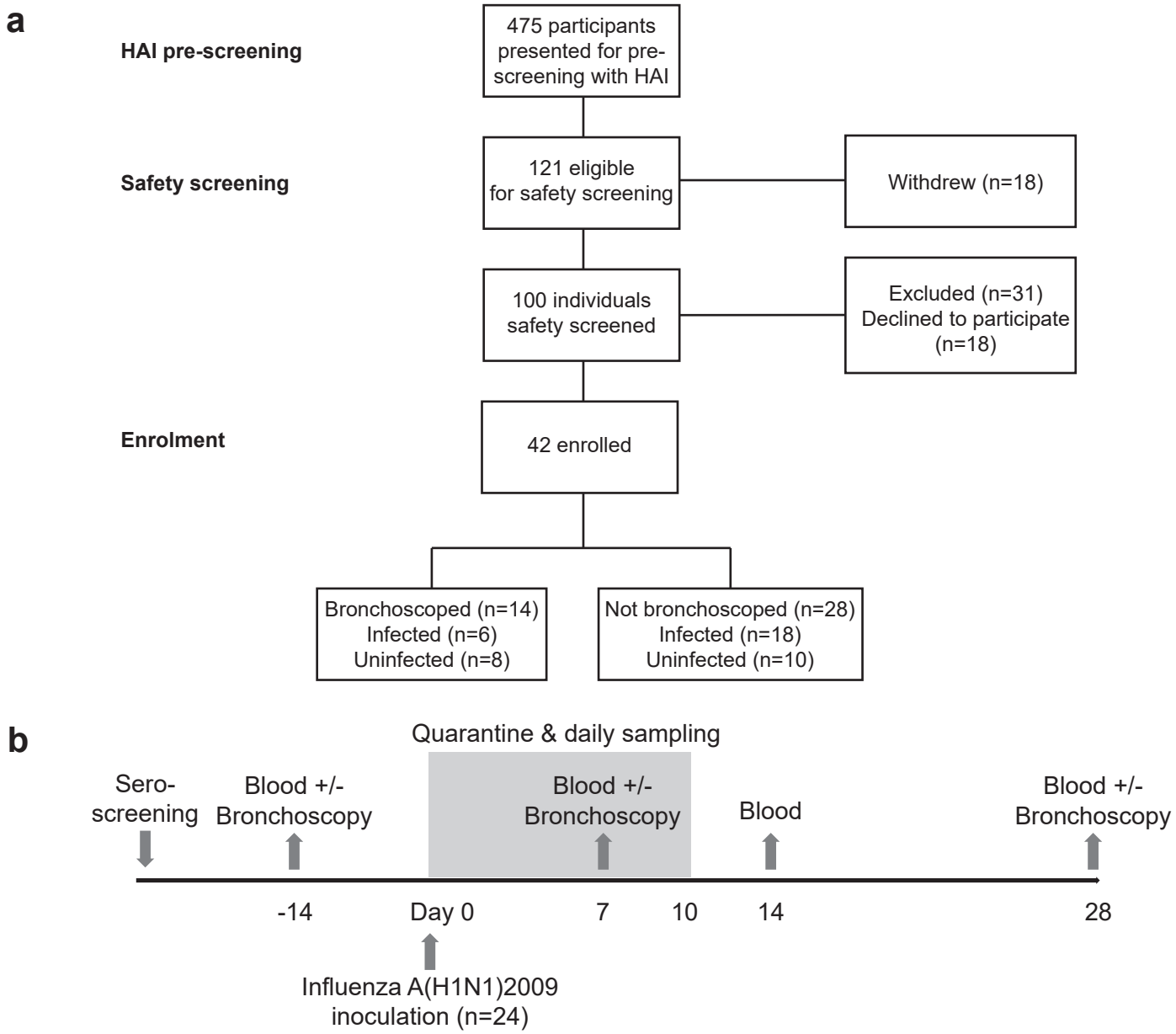

a
HAI pre-screening
475 participants presented for pre-screening with HAI
Safety screening
121 eligible for safety screening
Withdrew (n=18)
100 individuals safety screened
Excluded (n=31)
Declined to participate (n=18)
Enrolment
42 enrolled
Bronchoscoped (n=14)
Infected (n=6)
Uninfected (n=8)
Not bronchoscoped (n=28)
Infected (n=18)
Uninfected (n=10)
b
Quarantine & daily sampling
Sero-screening
Blood +/- Bronchoscopy
Blood +/- Bronchoscopy
Blood
Blood +/- Bronchoscopy
-14
Day 0
7
10
14
28
Influenza A(H1N1)2009 inoculation (n=24)
c
Mean VL
Nasal viral load (log10 copies/ml)
Day post inoculation
d
Infected
Non-infected
Total Symptom Score
Day post-inoculation
e
Systemic
Upper tract
Lower tract
Total Symptom Score
Day post inoculation

Figure 2

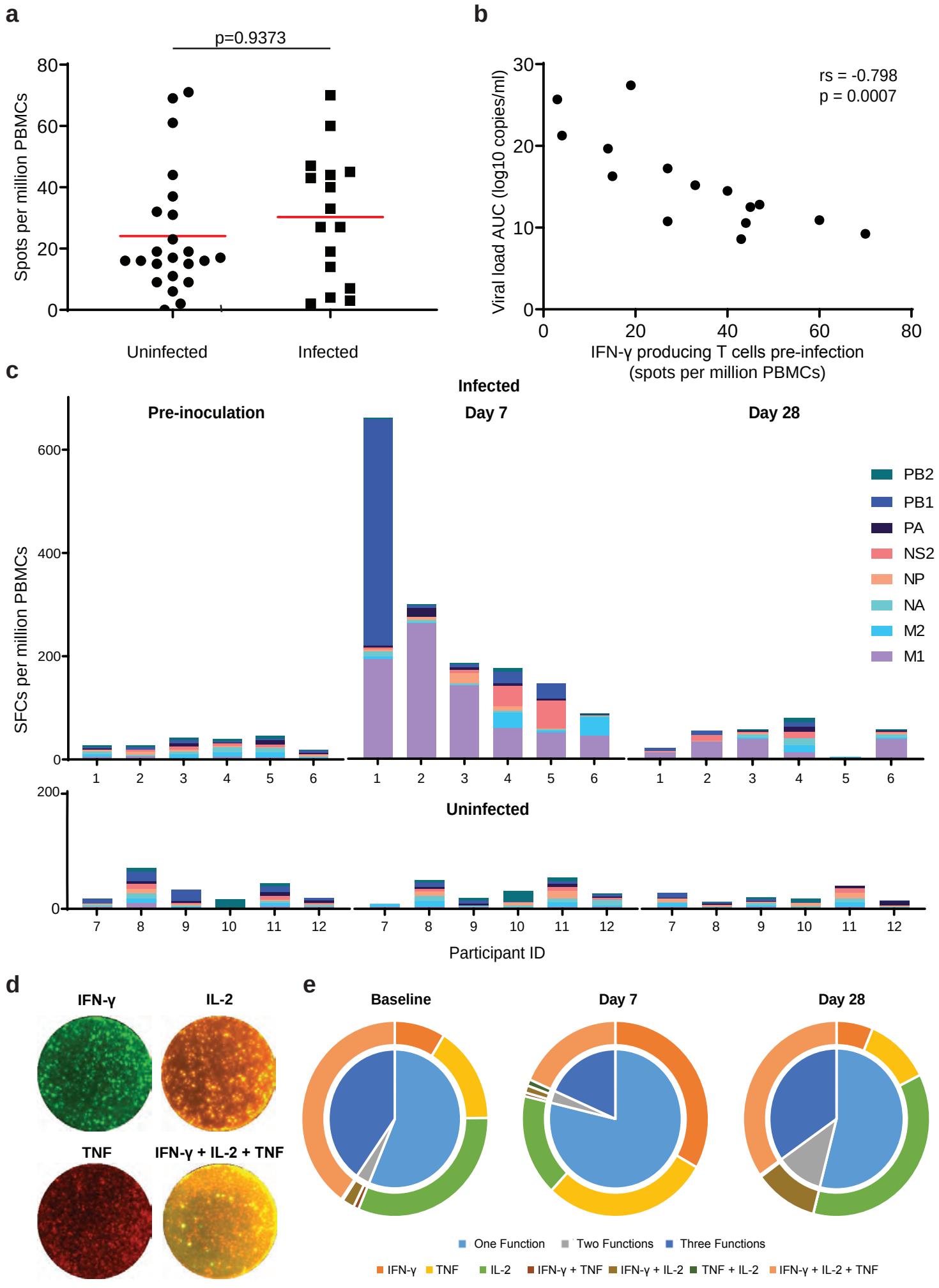

a
p=0.9373
Spots per million PBMCs
80
60
40
20
0
Uninfected
Infected
b
rs = -0.798
p = 0.0007
Viral load AUC (log10 copies/ml)
30
20
10
0
0
20
40
60
80
IFN-γ producing T cells pre-infection
(spots per million PBMCs)
c
Infected
Pre-inoculation
Day 7
Day 28
SFCs per million PBMCs
600
400
200
0
PB2
PB1
PA
NS2
NP
NA
M2
M1
1 2 3 4 5 6
Uninfected
7 8 9 10 11 12
Participant ID
d
IFN-γ
IL-2
TNF
IFN-γ + IL-2 + TNF
e
Baseline
Day 7
Day 28
One Function
Two Functions
Three Functions
IFN-γ
TNF
IL-2
IFN-γ + TNF
IFN-γ + IL-2
TNF + IL-2
IFN-γ + IL-2 + TNF

Figure 3

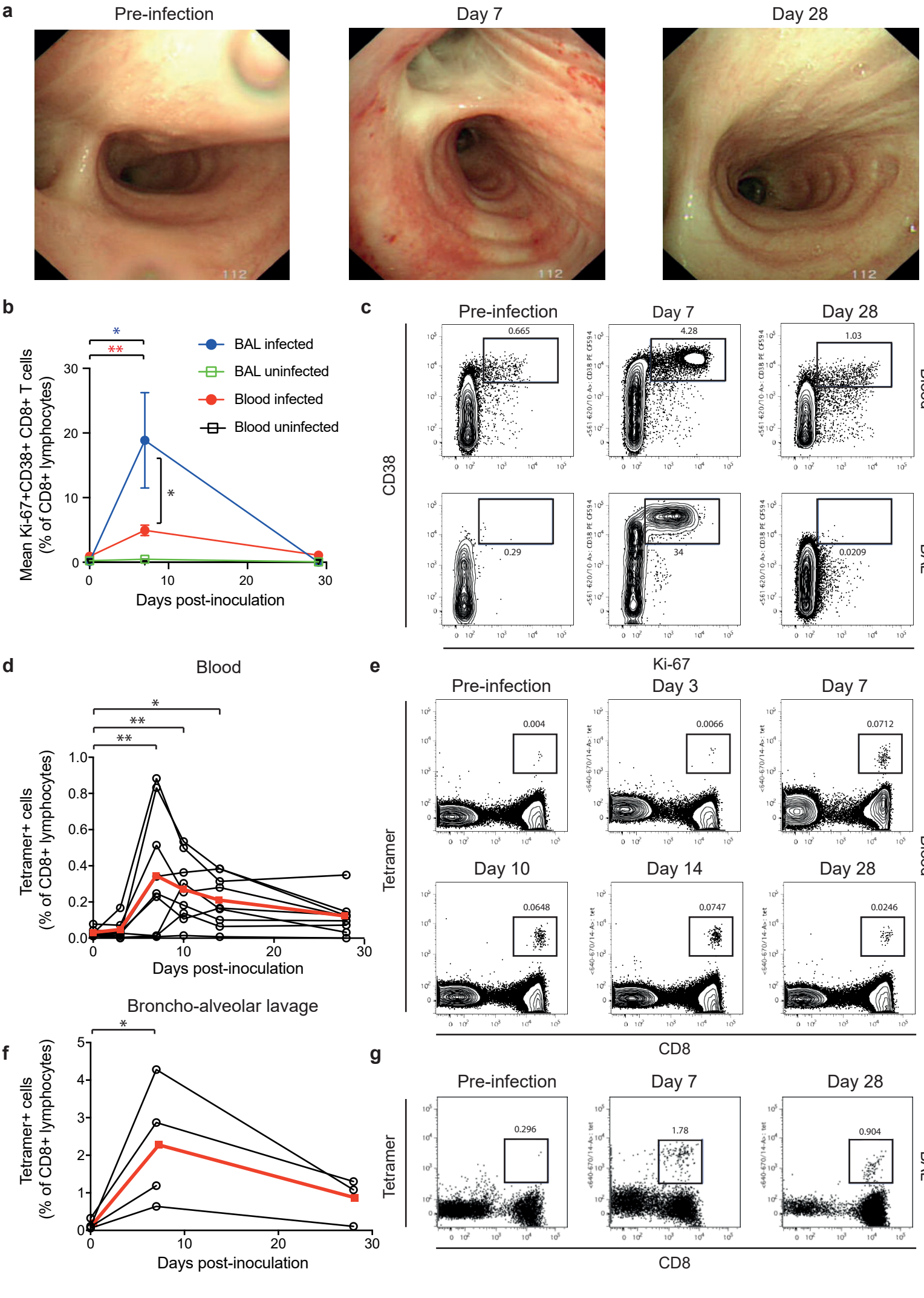

a
Pre-infection
Day 7
Day 28
b
Mean Ki-67+CD38+ CD8+ T cells (% of CD8+ lymphocytes)
BAL infected
BAL uninfected
Blood infected
Blood uninfected
Days post-inoculation
c
Pre-infection
Day 7
Day 28
0.665
4.28
1.03
0.29
34
0.0209
CD38
Ki-67
Blood
BAL
d
Blood
Tetramer+ cells (% of CD8+ lymphocytes)
Days post-inoculation
e
Pre-infection
Day 3
Day 7
Day 10
Day 14
Day 28
0.004
0.0066
0.0712
0.0648
0.0747
0.0246
Tetramer
CD8
f
Broncho-alveolar lavage
Tetramer+ cells (% of CD8+ lymphocytes)
Days post-inoculation
g
Pre-infection
Day 7
Day 28
0.296
1.78
0.904
Tetramer
CD8
BAL

Figure 4

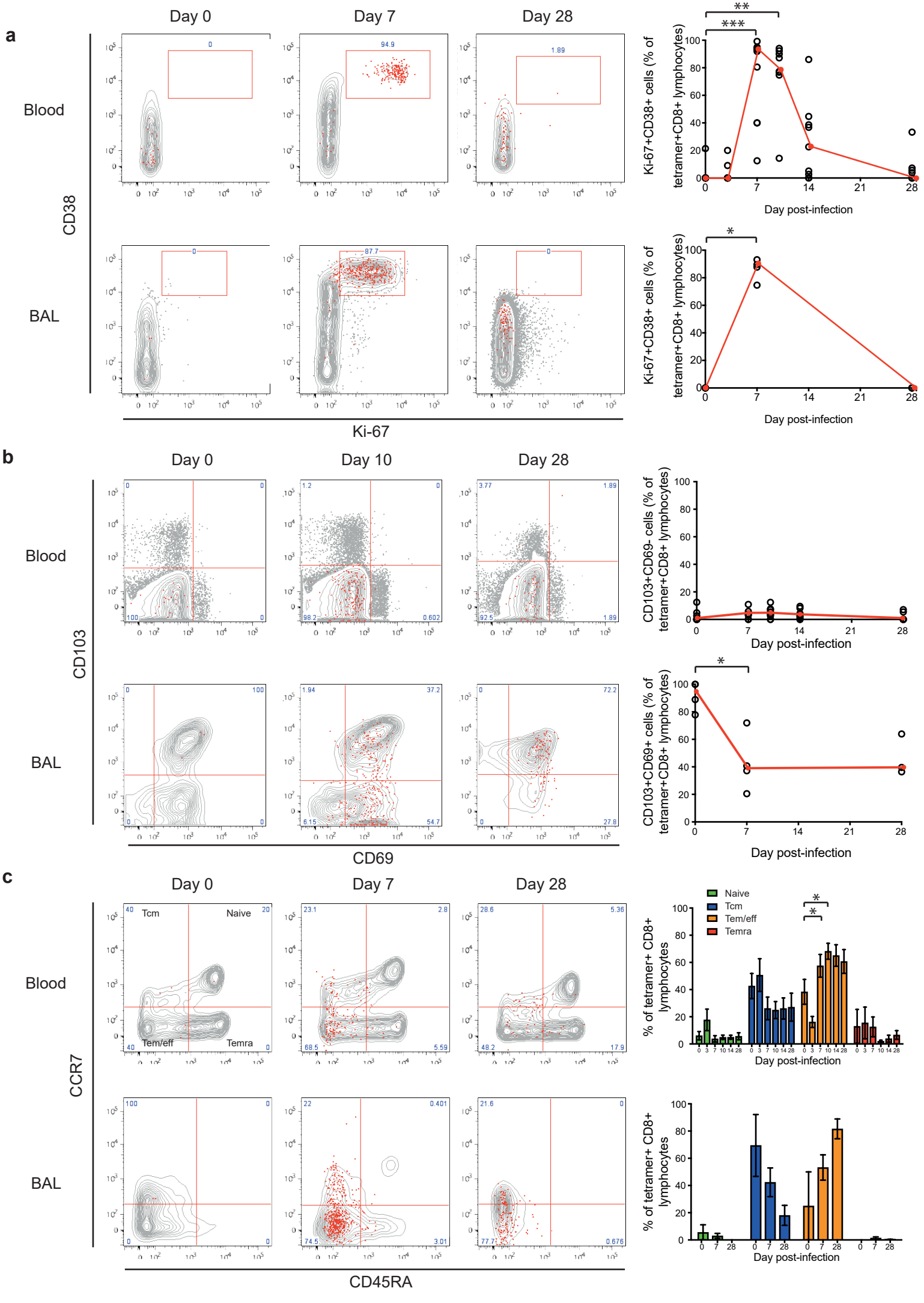

a
Day 0
Day 7
Day 28
Blood
BAL
CD38
Ki-67
94.9
1.89
87.7
Ki-67+CD38+ cells (% of tetramer+CD8+ lymphocytes)
Day post-infection
b
Day 0
Day 10
Day 28
CD103
CD69
CD103+CD69- cells (% of tetramer+CD8+ lymphocytes)
CD103+CD69+ cells (% of tetramer+CD8+ lymphocytes)
c
Tcm
Naive
Tem/eff
Temra
CCR7
CD45RA
Naive
Tcm
Tem/eff
Temra
% of tetramer+ CD8+ lymphocytes

Figure 4

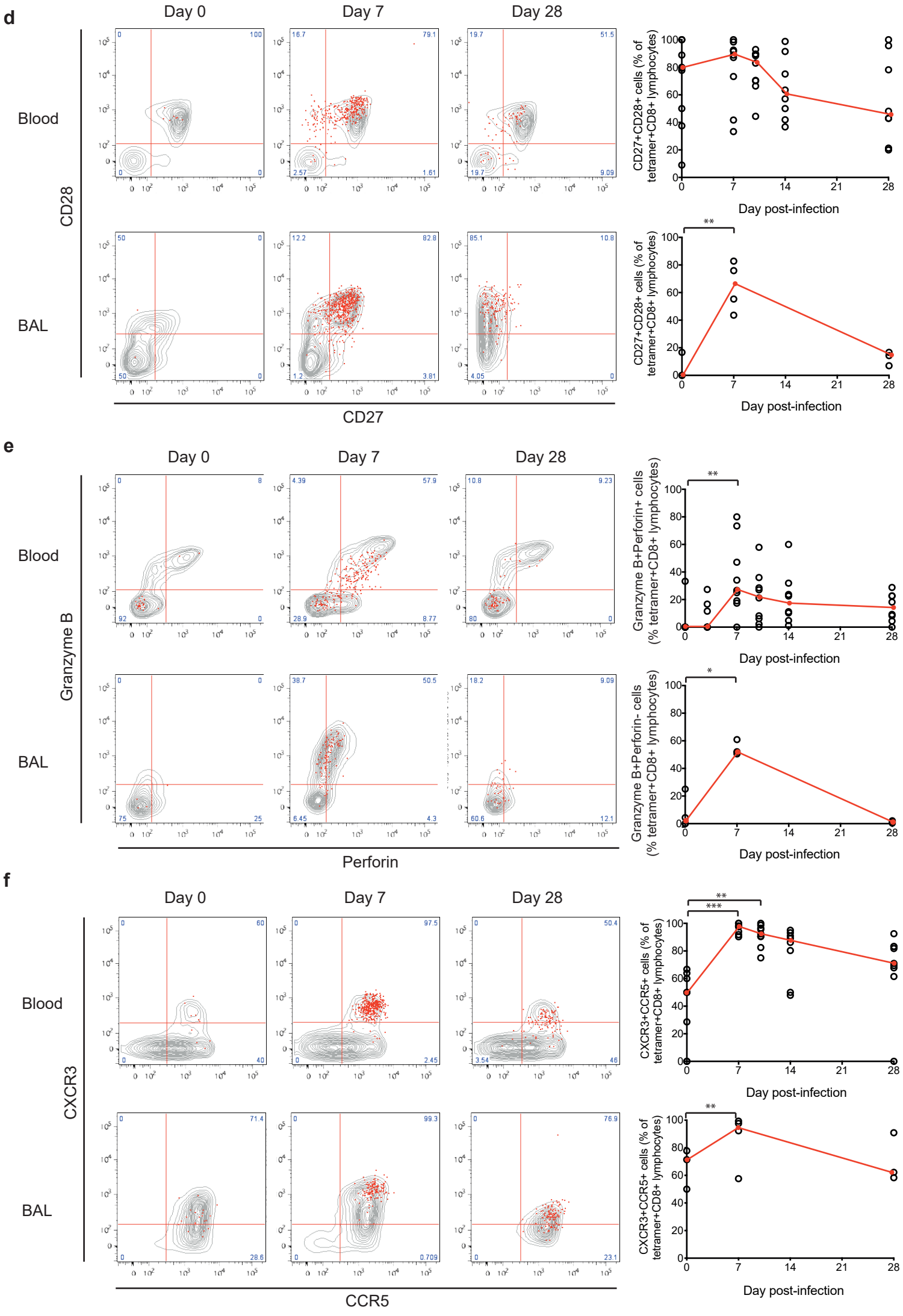

d
Day 0
Day 7
Day 28
Blood
BAL
CD28
CD27
CD27+CD28+ cells (% of tetramer+CD8+ lymphocytes)
Day post-infection
**
e
Granzyme B
Perforin
Granzyme B+Perforin+ cells (% tetramer+CD8+ lymphocytes)
Granzyme B+Perforin- cells (% tetramer+CD8+ lymphocytes)
*
f
CXCR3
CCR5
CXCR3+CCR5+ cells (% of tetramer+CD8+ lymphocytes)
***

Figure 5

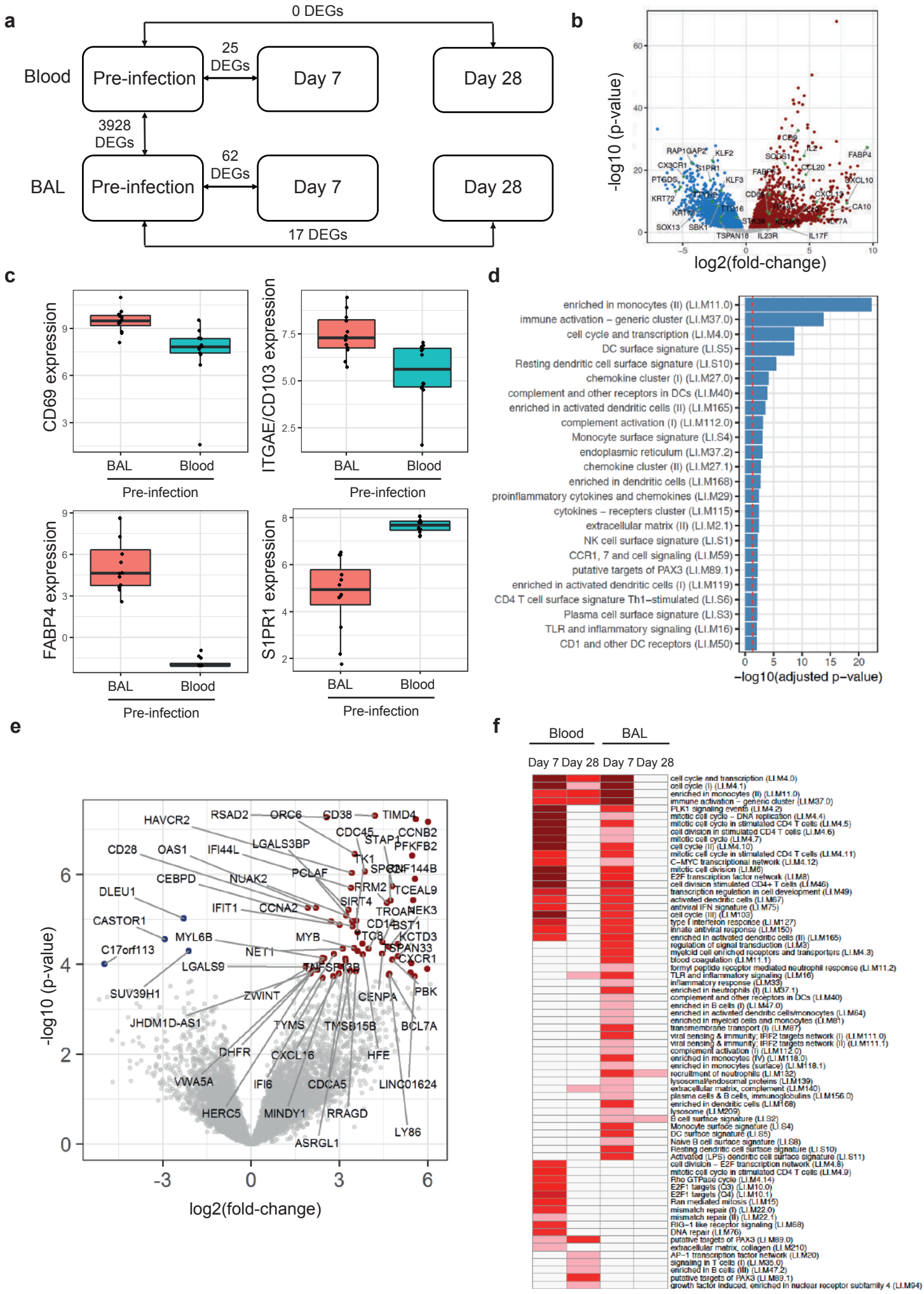
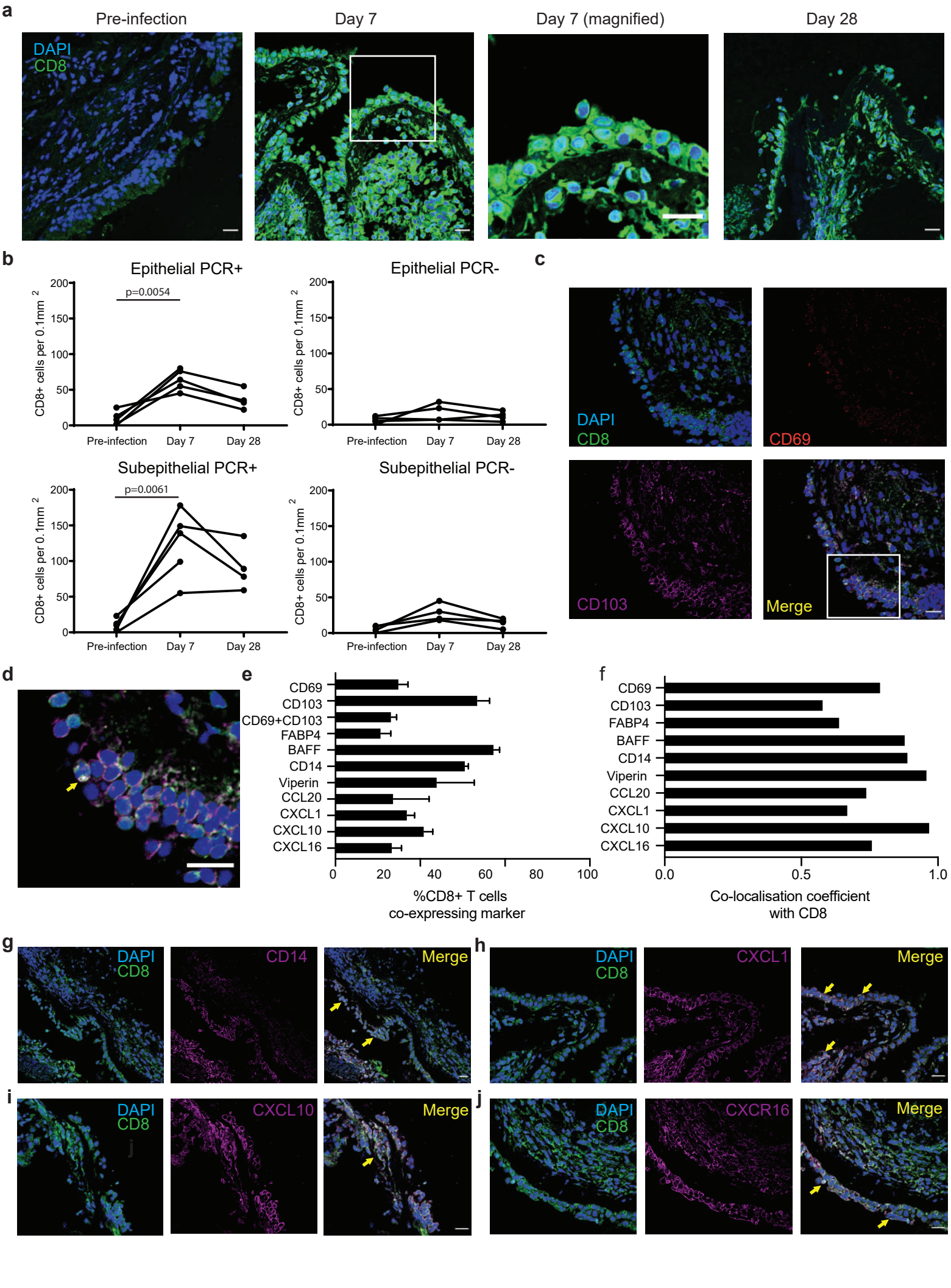
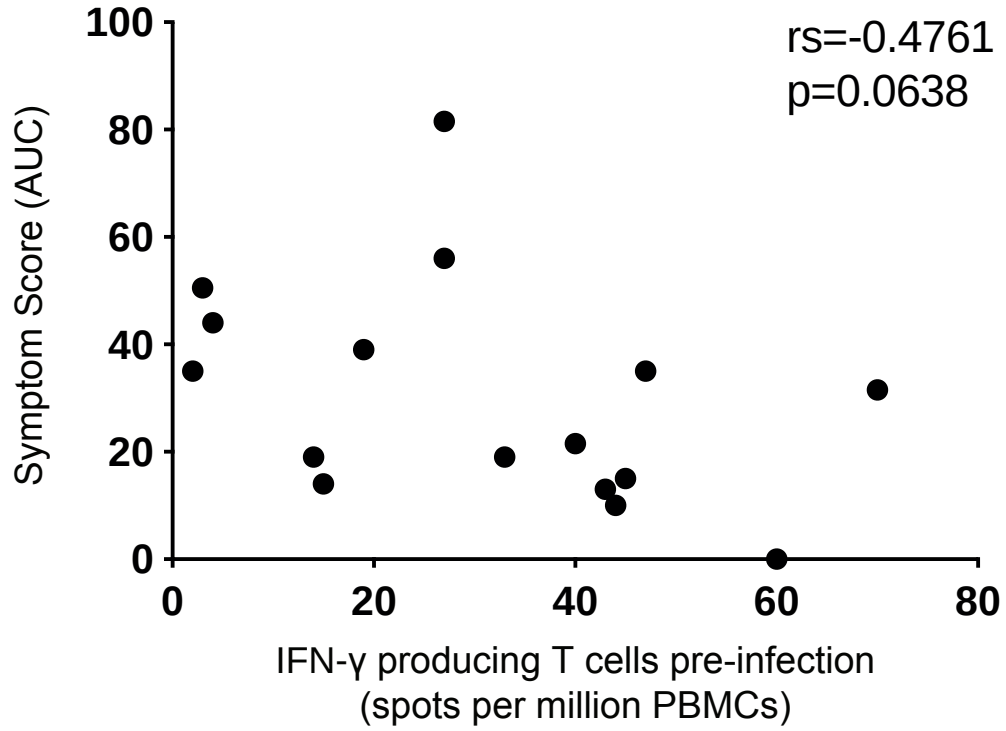

a
0 DEGs
Blood
Pre-infection
25 DEGs
Day 7
Day 28
3928 DEGs
BAL
Pre-infection
62 DEGs
Day 7
Day 28
17 DEGs
b
-log10 (p-value)
log2(fold-change)
c
CD69 expression
ITGAE/CD103 expression
FABP4 expression
S1PR1 expression
BAL
Blood
Pre-infection
d
enriched in monocytes (II) (LI.M11.0)
immune activation – generic cluster (LI.M37.0)
cell cycle and transcription (LI.M4.0)
DC surface signature (LI.S5)
Resting dendritic cell surface signature (LI.S10)
chemokine cluster (I) (LI.M27.0)
complement and other receptors in DCs (LI.M40)
enriched in activated dendritic cells (II) (LI.M165)
complement activation (I) (LI.M112.0)
Monocyte surface signature (LI.S4)
endoplasmic reticulum (LI.M37.2)
chemokine cluster (II) (LI.M27.1)
enriched in dendritic cells (LI.M168)
proinflammatory cytokines and chemokines (LI.M29)
cytokines – recepters cluster (LI.M115)
extracellular matrix (II) (LI.M2.1)
NK cell surface signature (LI.S1)
CCR1, 7 and cell signaling (LI.M59)
putative targets of PAX3 (LI.M89.1)
enriched in activated dendritic cells (I) (LI.M119)
CD4 T cell surface signature Th1–stimulated (LI.S6)
Plasma cell surface signature (LI.S3)
TLR and inflammatory signaling (LI.M16)
CD1 and other DC receptors (LI.M50)
–log10(adjusted p–value)
e
-log10 (p-value)
log2(fold-change)
f
Blood
BAL
Day 7 Day 28 Day 7 Day 28
cell cycle and transcription (LI.M4.0)
cell cycle (I) (LI.M4.1)
enriched in monocytes (II) (LI.M11.0)
immune activation – generic cluster (LI.M37.0)
PLK1 signaling events (LI.M4.2)
mitotic cell cycle – DNA replication (LI.M4.4)
mitotic cell cycle in stimulated CD4 T cells (LI.M4.5)
cell division in stimulated CD4 T cells (LI.M4.6)
mitotic cell cycle (LI.M4.7)
cell cycle (II) (LI.M4.10)
mitotic cell cycle in stimulated CD4 T cells (LI.M4.11)
C–MYC transcriptional network (LI.M4.12)
mitotic cell division (LI.M6)
E2F transcription factor network (LI.M8)
cell division stimulated CD4+ T cells (LI.M46)
transcription regulation in cell development (LI.M49)
activated dendritic cells (LI.M67)
antiviral IFN signature (LI.M75)
cell cycle (III) (LI.M103)
type I interferon response (LI.M127)
innate antiviral response (LI.M150)
enriched in activated dendritic cells (II) (LI.M165)
regulation of signal transduction (LI.M3)
myeloid cell enriched receptors and transporters (LI.M4.3)
blood coagulation (LI.M11.1)
formyl peptide receptor mediated neutrophil response (LI.M11.2)
TLR and inflammatory signaling (LI.M16)
inflammatory response (LI.M33)
enriched in neutrophils (I) (LI.M37.1)
complement and other receptors in DCs (LI.M40)
enriched in B cells (I) (LI.M47.0)
enriched in activated dendritic cells/monocytes (LI.M64)
enriched in myeloid cells and monocytes (LI.M81)
transmembrane transport (I) (LI.M87)
viral sensing & immunity: IRF2 targets network (I) (LI.M111.0)
viral sensing & immunity: IRF2 targets network (II) (LI.M111.1)
complement activation (I) (LI.M112.0)
enriched in monocytes (IV) (LI.M118.0)
enriched in monocytes (surface) (LI.M118.1)
recruitment of neutrophils (LI.M132)
lysosomal/endosomal proteins (LI.M139)
extracellular matrix, complement (LI.M140)
plasma cells & B cells, immunoglobulins (LI.M156.0)
enriched in dendritic cells (LI.M168)
lysosome (LI.M209)
B cell surface signature (LI.S2)
Monocyte surface signature (LI.S4)
DC surface signature (LI.S5)
Naive B cell surface signature (LI.S8)
Resting dendritic cell surface signature (LI.S10)
Activated (LPS) dendritic cell surface signature (LI.S11)
cell division – E2F transcription network (LI.M4.8)
mitotic cell cycle in stimulated CD4 T cells (LI.M4.9)
Rho GTPase cycle (LI.M4.14)
E2F1 targets (Q3) (LI.M10.0)
E2F1 targets (Q4) (LI.M10.1)
Ran mediated mitosis (LI.M15)
mismatch repair (I) (LI.M22.0)
mismatch repair (II) (LI.M22.1)
RIG–1 like receptor signaling (LI.M68)
DNA repair (LI.M76)
putative targets of PAX3 (LI.M89.0)
extracellular matrix, collagen (LI.M210)
AP–1 transcription factor network (LI.M20)
signaling in T cells (I) (LI.M35.0)
enriched in B cells (III) (LI.M47.2)
putative targets of PAX3 (LI.M89.1)
growth factor induced, enriched in nuclear receptor subfamily 4 (LI.M94)

Figure 6

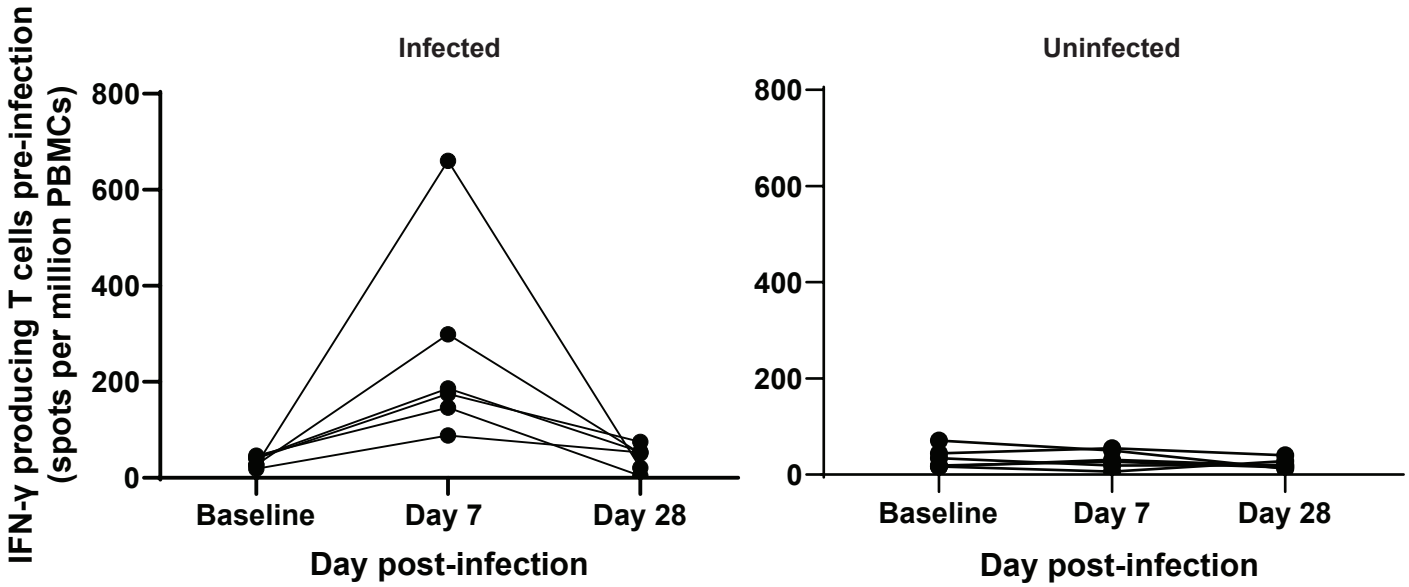

a
Pre-infection
Day 7
Day 7 (magnified)
Day 28
DAPI
CD8
b
Epithelial PCR+
Epithelial PCR-
Subepithelial PCR+
Subepithelial PCR-
p=0.0054
p=0.0061
CD8+ cells per 0.1mm 2
Pre-infection
Day 7
Day 28
c
DAPI
CD8
CD69
CD103
Merge
d
e
CD69
CD103
CD69+CD103
FABP4
BAFF
CD14
Viperin
CCL20
CXCL1
CXCL10
CXCL16
%CD8+ T cells
co-expressing marker
f
Co-localisation coefficient
with CD8
g
CD14
h
CXCL1
i
CXCL10
j
CXCR16

Supplementary Figure 1

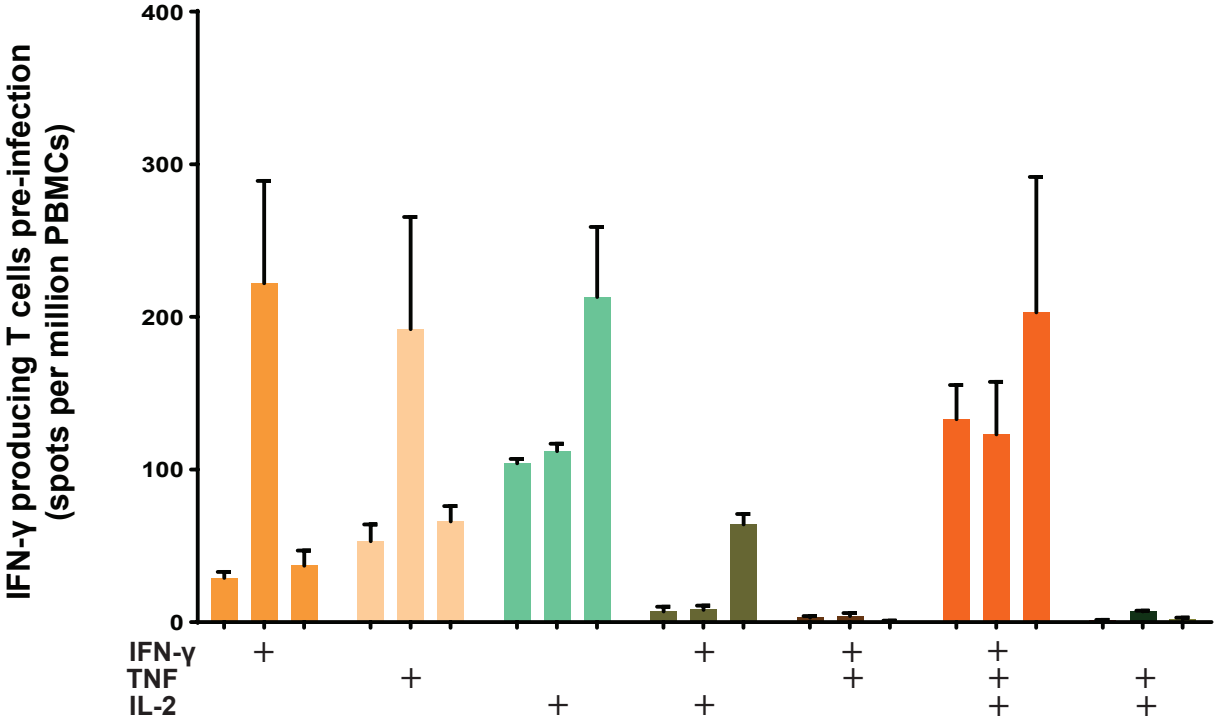
a



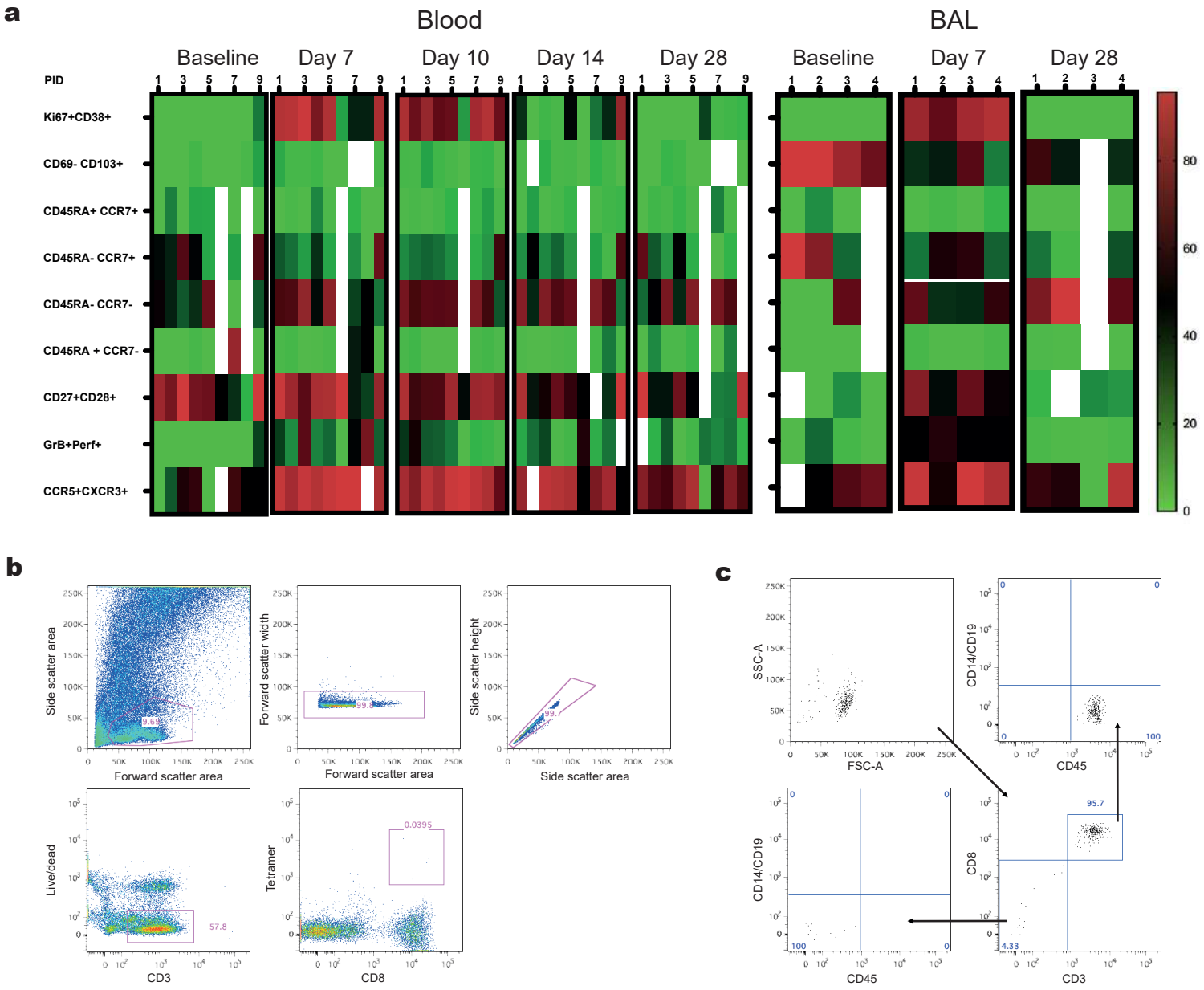
b



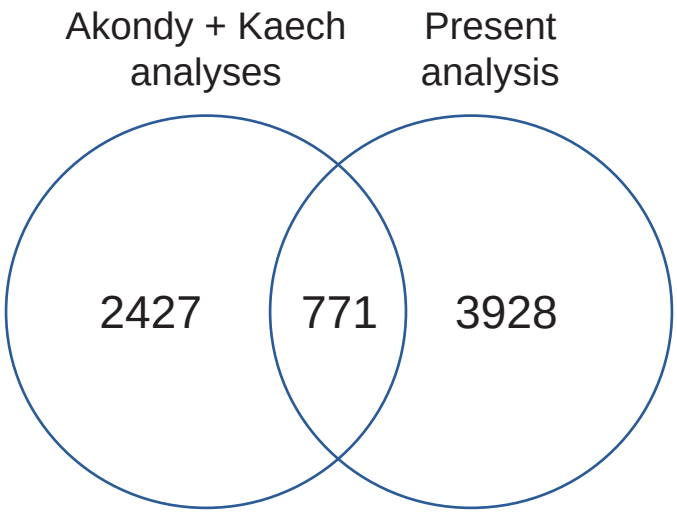
Supplementary Figure 2



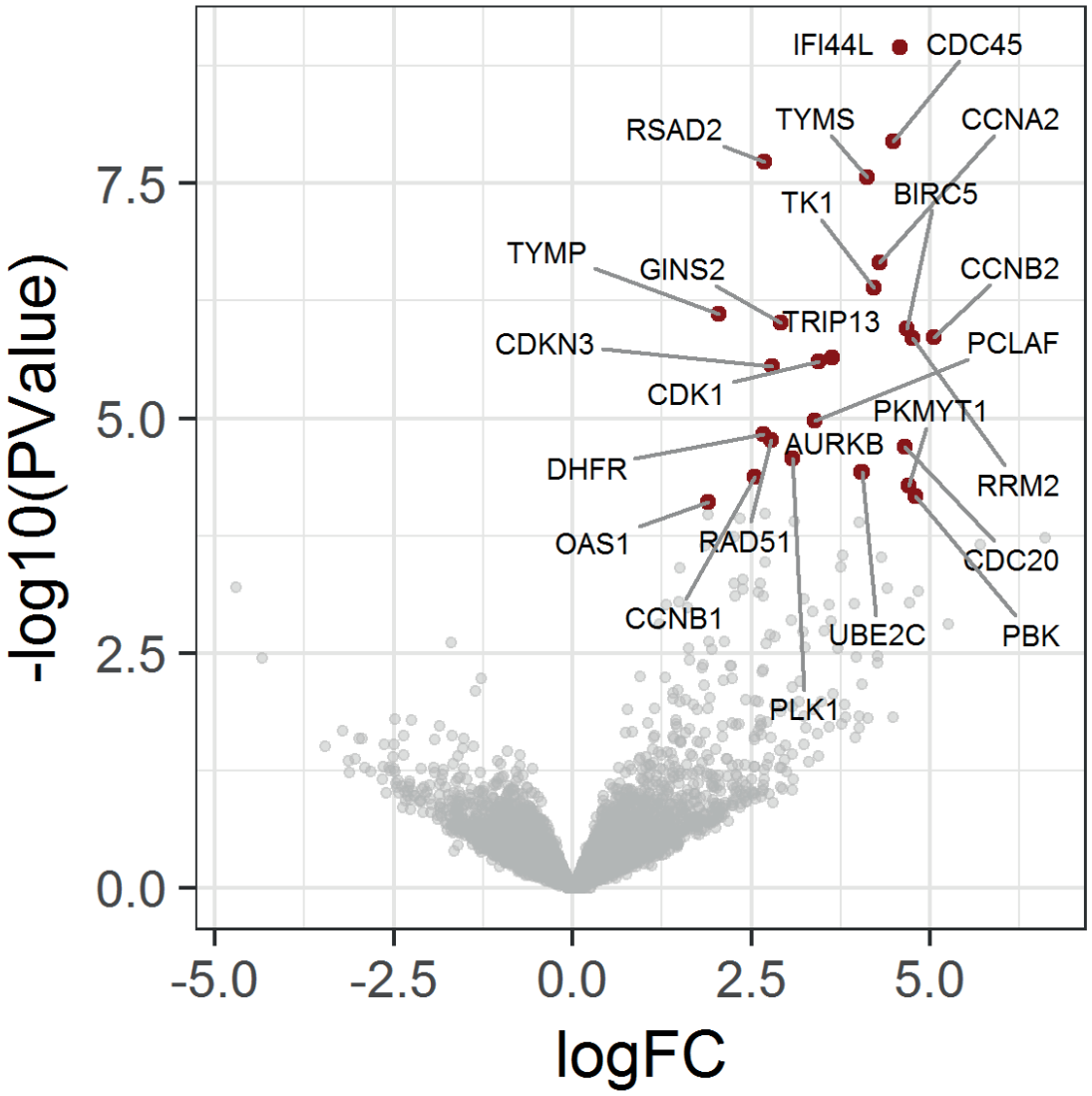
Supplementary Figure 3



Supplementary Figure 4



Supplementary Figure 5



Supplementary Figure 6

